

Sensor and Simulation Notes

Note 507

December 2005

A High-Voltage Cable-Fed Impulse Radiating Antenna

Leland H. Bowen and Everett G. Farr
Farr Research, Inc.

William D. Prather
Air Force Research Laboratory, Directed Energy Directorate

Abstract:

We describe here a 1.52 m (5 ft.) diameter Impulse Radiating Antenna (IRA) for use in a high-voltage radar system that uses a single antenna and a directional coupler. This antenna, designated the IRA-6, was designed to operate at 30 kV. To accommodate the higher voltage, we introduced a number of new features, including a larger-diameter 100-ohm cable, cable stubs at the feed point, and gaps in the splitter balun. These features led to somewhat higher reflections in the TDR and somewhat reduced gain. However, the realized gain was satisfactory as high as 4 GHz, which covered the frequencies of interest. We tested the antenna at low, medium and high voltages, for which we provide results. The peak gain on boresight is 20 dBi at 3.1 GHz and the effective height is approximately 0.187 m.

I. Introduction

We describe here a high-voltage cable-fed Impulse Radiating Antenna (IRA) that was developed as part of an Ultra-Wideband (UWB) radar system using a single antenna and a directional coupler [1]. In this configuration, it is not possible to use a sharpening switch at the apex to handle high voltages, so we investigated using higher voltages on a standard IRA with splitter balun. The resulting antenna, referred to as the IRA-6, was built and tested at three different voltage levels.

This antenna is intended to be operated with a pulser with 30 kV peak voltage, 150 ps risetime, 3 ns pulse duration (at $1/e$ of peak), and 1 kHz maximum pulse repetition frequency (PRF) (manufacturer's specs.). To prevent flashover at this voltage level, we incorporated a number of compromises into the antenna design at the splitter and feed point (focus), which led to somewhat larger reflections in the TDR than we are accustomed to seeing. These compromises also led to reduced realized gain, especially at higher frequencies. Nevertheless, the IRA-6 performed quite well as high as 4 GHz, which met the requirements for the radar system under study.

II. Description of the IRA-6

The IRA-6 is 1.52 m (5 ft.) in diameter, with a focal length of 0.56 m ($F/D = 0.37$). It has feed arms positioned at $\pm 45^\circ$ to the vertical, and it is manufactured from a spun aluminum reflector. It includes a ground plane in the horizontal plane of symmetry, which adds structural rigidity and reduces crosspol, as described in [2]. A photo of the IRA-6 is shown in Figure 2.1.

The feed arms and ground plane were fabricated from aluminum honeycomb sheets produced by Teklam to reduce weight. This reduced the stress on the cable connections at the feed point (focus), which are sensitive to shock and vibration. The honeycomb sheets are 6.3 mm (0.25 in) thick with 0.5 mm (0.020 in) thick surfaces on each side of the honeycomb material. This provides approximately 80% of the strength of solid aluminum at approximately 20% of the weight. The edges of the honeycomb material were covered with copper tape to maintain electrical continuity between the two sides.

A new feature of the antenna is the high-voltage splitter balun, show in Figure 2.2. This uses a custom cable that is roughly equivalent to RG-213 in diameter, with a narrower center conductor to realize a 100 Ω impedance. An HN-Type panel-mount connector is used at the input port. The insulation on connector and the ends of the 100- Ω cables are both tapered, which is apparent on the right in Figure 2.2. The walls of the aluminum housing are also tapered, but in the reverse direction, to increase the high-voltage standoff between the center conductor and the housing wall. The minimum distance between the center conductors and the housing walls is 3.6 mm and the path length along the surface of the tapered dielectric is 19 – 21 mm.

The void inside the splitter is filled with Jet-Lube silicon dielectric compound DM-3, which has a dielectric strength of 20 kV/mm (500 V/mil). This was selected because it is available in a cartridge for a standard automotive type grease gun. This allows one to inject the

compound under considerable pressure to completely fill the void. The tapers on the insulators and the inside walls of the splitter were designed to maintain a constant impedance, based on dielectric constants of 2.9 for the DM-3, 2.25 for the polyethylene insulation in the 100 Ω cable, and 2.1 for the TFE insulation in the HN-Type connector. We were unable to locate an accurate dielectric constant for the DM-3, so we used the value of 2.9, because this is typical for silicone compounds at low frequency. Note that dielectric constants are seldom specified at frequencies above 1 MHz, so accurate information is generally difficult to obtain. We show the splitter and feed cables on the back side of the IRA-6 in Figure 2.3.



Figure 2.1. Front view of the IRA-6.

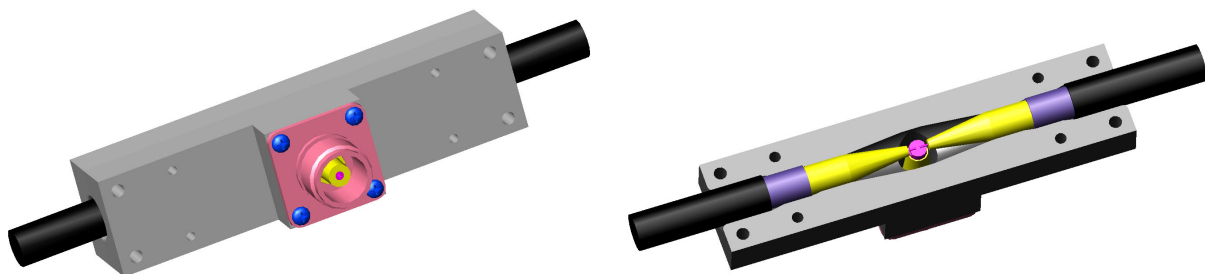


Figure 2.2. High voltage splitter, front (left), back removed (right).



Figure 2.3. Splitter with feed cables mounted on back side of IRA-6.

At the feed point are two cable stubs that are 19 mm (0.75 in.) in length, to prevent flashover. Three close-up views of the feed point are shown in Figure 2.4. The tight bend at the tip of the bottom cable was formed by warming the dielectric with a heat gun, bending the insulation to the required shape, and allowing the plastic to cool.

The high-voltage splitter consists of two cables of equal length, connected in parallel at the connector and in series at the focus. We found it necessary to tune the cable lengths by measuring the time of arrival of the pulse on either side of the ground plane with a home-made sensor. The sensor was a semi-rigid cable with center conductor protruding and bent at an angle of 90 degrees. It was carefully placed at the same position on either side of the ground plane, to obtain an accurate time of arrival for the main pulse.

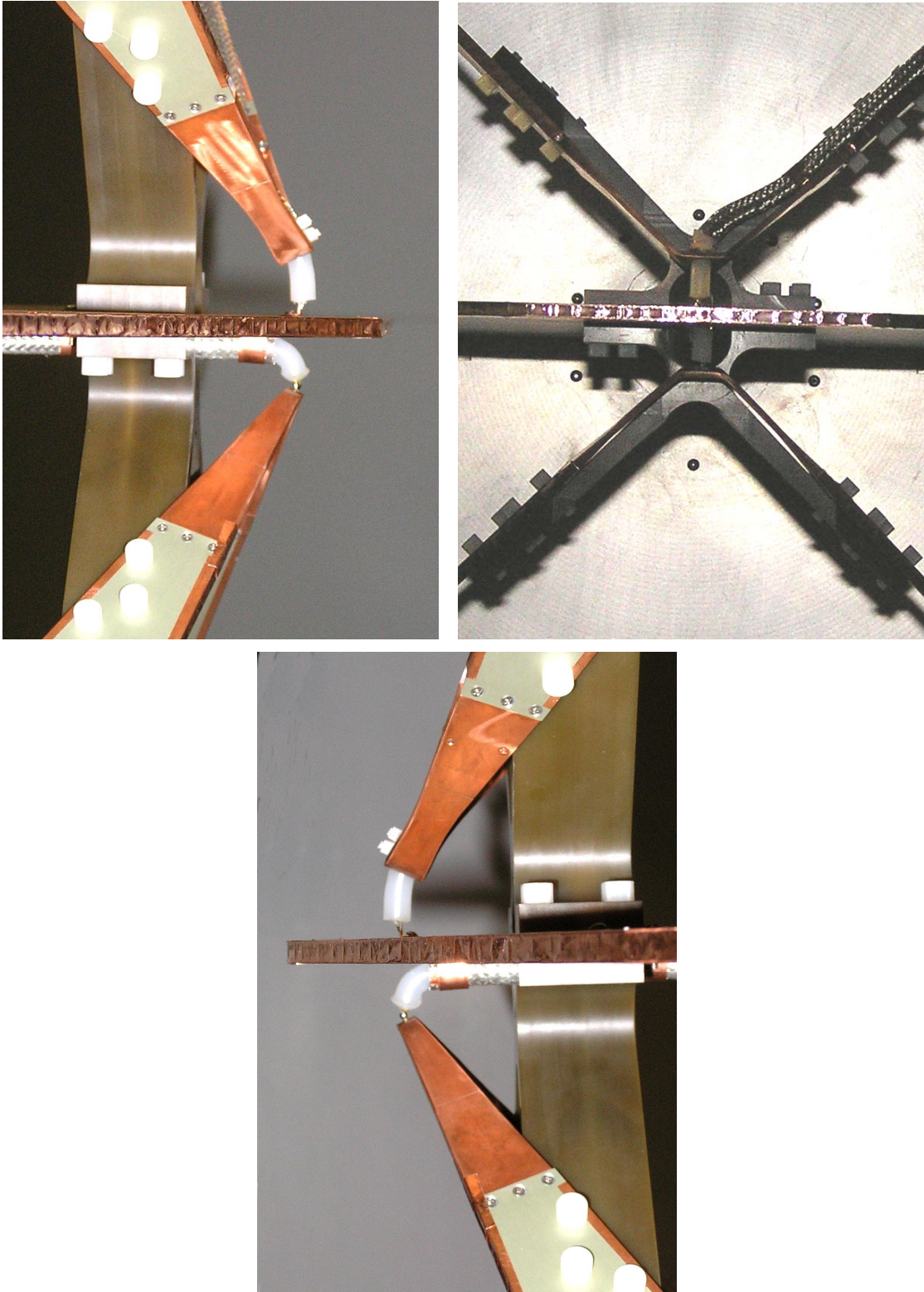


Figure 2.4. IRA-6 feed point from the left (upper left), front (upper right), and right (bottom).

The resistive load consists of seven strings of 2-watt metal film resistors, as shown in Figure 2.5. The material supporting the resistors at the end of the feed arms is polycarbonate (Lexan®) with a thickness of 5 mm (3/16 in.) that has been drilled with many holes to reduce the capacitance at the end of the feed arms. The feed cable is routed away from the load resistors and has five ferrite beads to prevent shorting out the load resistors.

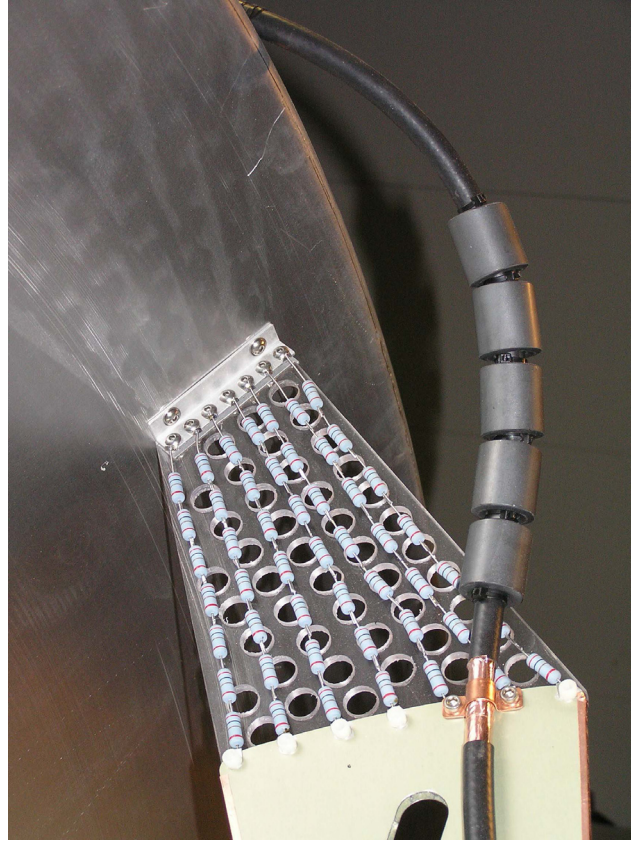


Figure 2.5. Detail of the load resistors and ferrite beads on feed cable.

III. Low-Voltage measurements

We first characterized the IRA-6 using a low voltage pulser on the Portable Automated Time-domain Antenna Range (*PATAR*[®]) developed by Farr Research. The pulser, a Picosecond Pulse Labs model 4015C, has a negative 4 V peak voltage with a rise time of approximately 20 ps. The pulser drove a Farr Research model TEM-1-50 sensor to form the transmit portion of the antenna range. The receive section of the range consisted of the IRA-6 connected to a Tektronix model TDS8000 digital sampling oscilloscope with a model 80E04 sampling head. The TEM-1-50 and the IRA-6 were supported approximately 3 m above the ground with the apertures spaced 20 m apart. This test configuration is capable of measurements as high as 20 GHz, which is considerably higher than the frequencies of interest for the IRA-6 system.

In Figure 3.1 we show the TDR of the IRA-6 on the left. The reflections at the splitter and feed point are due to the compromises we have made to accommodate high voltage standoff. The TDR of the splitter is not as good as expected, possibly due to voids in the dielectric gel. The TDR at the feed point was initially much worse, but we were able to improve the configuration considerably by tuning the cable lengths and bending the cable stubs. Reflections at the feed point may be a concern; because they may be reflected into the oscilloscope, causing either over-voltage and/or ghost images in a radar measurement.

The impedance match in the vicinity of the feed arm loads is quite good. We experimented with various cable placements near the resistors, testing whether the TDR could be improved by placing the cable farther away from the resistors. However, we found this made little difference.

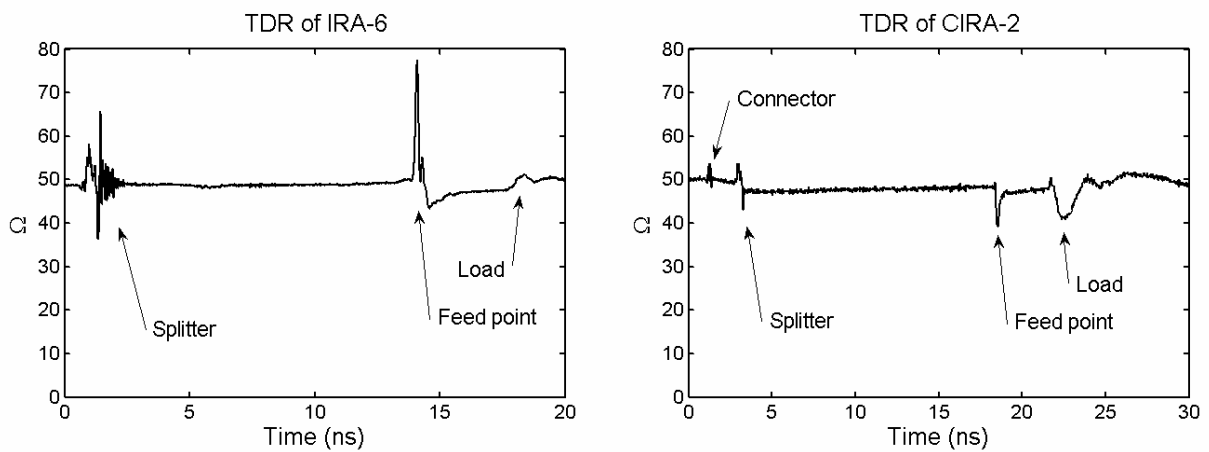


Figure 3.1. TDRs of the IRA-6 (left) and CIRA-2 (right).



Figure 3.2. Farr Research model CIRA-2.

In order to provide a point of comparison, we also provide data on the Farr Research model CIRA-2, which is a collapsible man-portable IRA, shown in Figure 3.2. The CIRA-2 is only a little smaller than the IRA-6 (1.22 m diameter instead of 1.5 m), so the comparisons should be useful. The CIRA-2 has an F/D of 0.4 and it has feed arms positioned at $\pm 30^\circ$ to vertical. The reflector and feed arms are fabricated from a conductive fabric, so the antenna can be folded into a compact lightweight package. The splitter is similar to that of the IRA-6, except that it is fabricated from a thinner and more flexible 95- Ω cable. Additional information on the CIRA-2 may be found in [3].

The TDR of the CIRA-2 is shown on the right in Figure 3.1. The CIRA-2 has no high voltage requirement, so the splitter and feed point are built much smaller than those on the IRA-6, resulting in a much flatter TDR. At the load, however, there is a larger dip than in the IRA-6. This is due to the fact that IRAs with feed arms positioned at $\pm 30^\circ$ should have loads concentrated at the edge of the feed arms, instead of being evenly distributed, as shown in [4]. However, distributed resistors are probably necessary in a collapsible IRA for practical reasons.

Next, we show the normalized impulse responses for the IRA-6 and CIRA-2 in Figure 3.3. The FWHM for the IRA-6 is much greater than that of the CIRA-2, due to the very wide gaps and insulated stubs required for high voltage operation. Depending on the operating voltage, it may be possible to improve the high frequency response of the IRA-6 by using shorter cable stubs at the feed point. One might also try machining ribs into the stubs to decrease the stub length while maintaining voltage standoff. However, this would eliminate the possibility of tuning the cable lengths to synchronize the response of the two antenna halves.

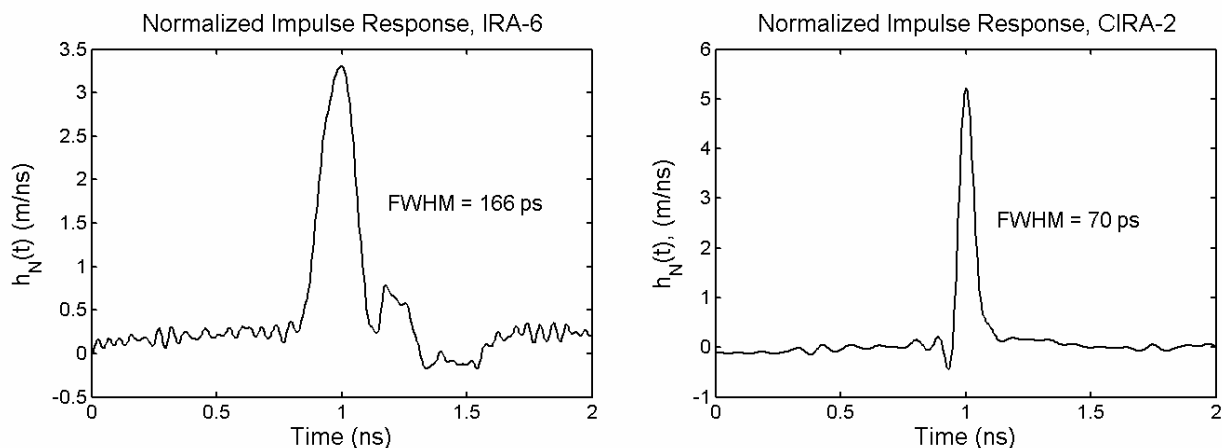


Figure 3.3. Normalized impulse response for the IRA-6 and the CIRA-2.

We can find the effective height of the antenna, h_{eff} , from the integral of the impulse response using [5, eqns A.2 and A.3]

$$h_{eff} = \sqrt{\frac{50 \Omega}{377 \Omega}} \int_{\text{Impulse}} h_N(t) dt \quad (3.1)$$

from which we measure $h_{eff} = 0.187$ m. If we ignore feed blockage, the theoretical effective height for a standard IRA with 200-ohm feed section can be calculated from [6] as

$$h_{eff} = \frac{a}{2\sqrt{2}} \quad (3.2)$$

so we expect $h_{eff} = 0.261$ m for the IRA-6. Thus, the measured effective height of the IRA-6 is about 71% of the theoretical value. An analogous quantity for the CIRA-2 is 62% of the theoretical value, probably due to the modest precision in the fabric reflector. We can also compare to the IRA-1, a solid reflector with feed arms positioned at $\pm 45^\circ$ to vertical with a diameter of 46 cm (18 in.), as described in [3]. Here, we find the analogous quantity is 74% of the expected value, which is a bit of an improvement over the IRA-6. This is probably due to the fact that the IRA-1 was designed for low voltage. Note that the above theoretical value for effective height does not include a factor that accounts for feed arm blockage, which was shown in [7, Figure 5.5] to reduce the value by a factor of 0.92. If we include this factor, the effective height of the IRA-6 would be 77% of the expected value, instead of 71%.

We show the realized gains for the IRA-6 and CIRA-2 in Figures 3.4 and 3.5. The gain of the IRA-6 drops off above 4 GHz due to the high-voltage design. However, below 2 GHz the gain of the IRA-6 is higher than that of the CIRA-2. This is expected, since the IRA-6 is larger in diameter by a factor of 1.25. This feature is illustrated quite clearly in Figure 3.5, where we show the realized gain only as high as 4 GHz. The peak realized gain of the IRA-6 is approximately 20 dBi at 3.12 GHz.

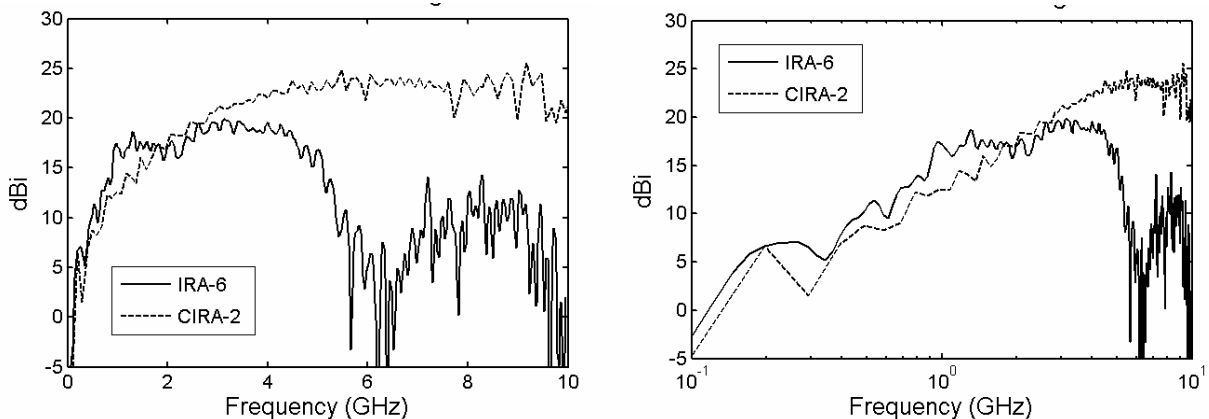


Figure 3.4. Realized gain on boresight for the IRA-6 and CIRA-2.

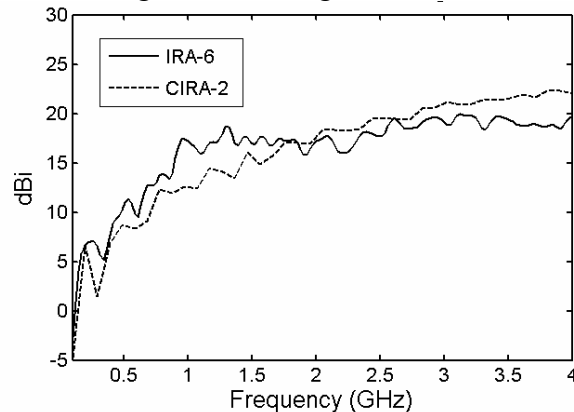


Figure 3.5. Realized Gain of the IRA-6 and CIRA-2.

The antenna patterns in the H- and E-planes are shown in Figure 3.6. These patterns are based on the peak value of the normalized impulse response. In Figure 3.7 we show the patterns of the IRA-6 based on gain as a function of frequency. There are some side lobes present but the pattern looks quite good below about 4 GHz.

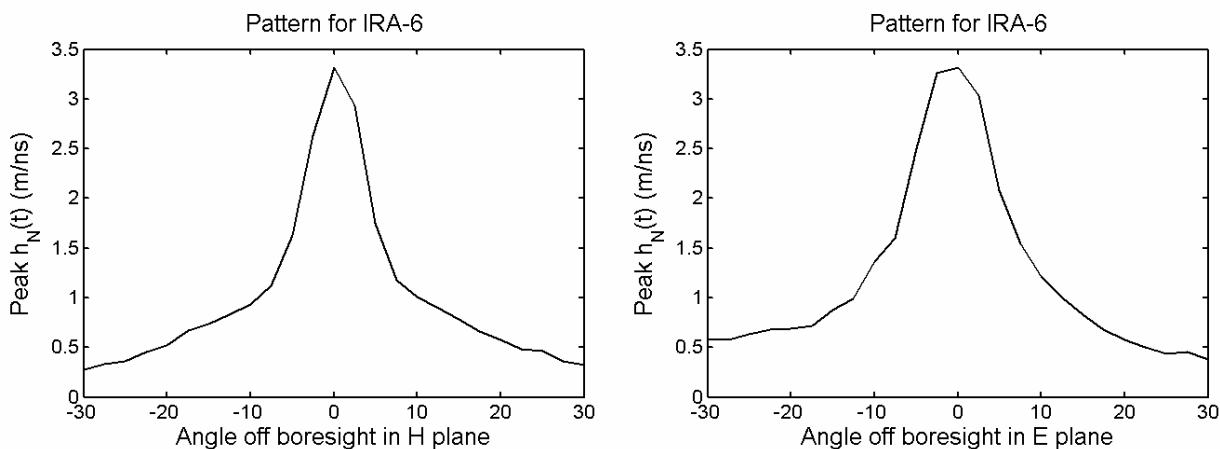


Figure 3.6. Antenna patterns for the IRA-6 based on peak impulse response, $h_N(t)$.

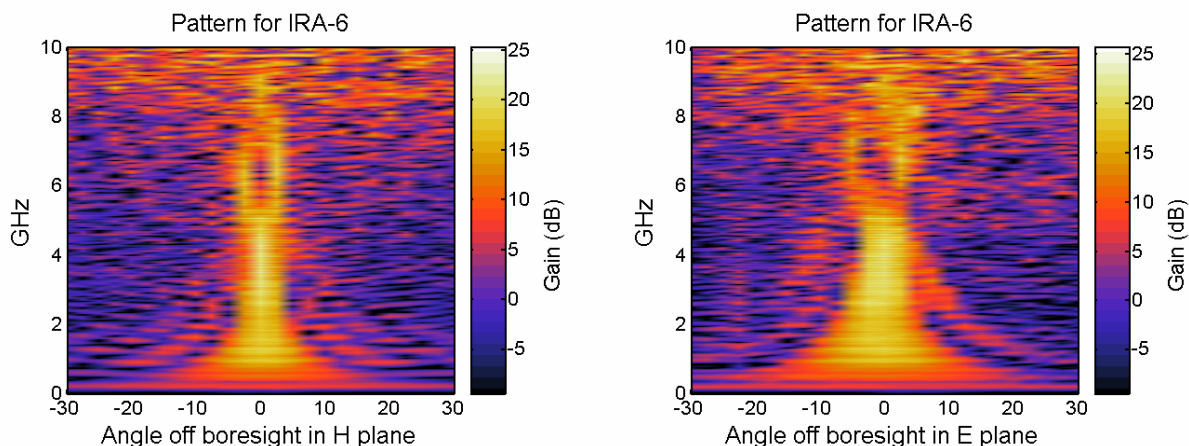


Figure 3.7. Antenna pattern of the IRA-6 based on gain.

IV. Mid-voltage measurements.

Next, we tested the IRA-6 with a Grant Applied Physics model HYPS pulser. The output of this pulser is a negative voltage pulse with a peak of -4.5kV . We show the inverted output of the HYPS in Figure 4.1. The output voltage rises (or falls) in two stages. First there is a very fast rise followed by a much slower section. This suggests that the 10-90% risetime is a poor measure of the speed of the pulser. Instead, we characterize the pulser in terms of the FWHM of the derivative of the output voltage. We show the derivative of the voltage in Figure 4.2, where we see that the FWHM is 139 ps. We drove the IRA-6 with the HYPS pulser and measured the field at a distance of 20.4 m. As expected, the IRA-6 handled the 4.5-kV pulse without flashover. The electric field was measured using a Farr Research model TEM-1-50 sensor connected to a

Tektronix model TDS 8000 digital sampling oscilloscope. The received voltage was converted to incident electric field using the effective height of the sensor h_{eff} and the equation [5, eqn. A.3]

$$V_{rec}(t) \approx h_{eff} E_{inc}(t) \quad (4.1)$$

For the TEM-1-50, h_{eff} is 0.018 m. We repeat the output of the HYPS with the same time scale used to measure the E-field in Figure 4.3. The E-field is shown in Figure 4.4, where we see that the peak field is approximately 600 V/m. There is some pre-pulse noise from the HYPS that becomes apparent in the E-field measurement.

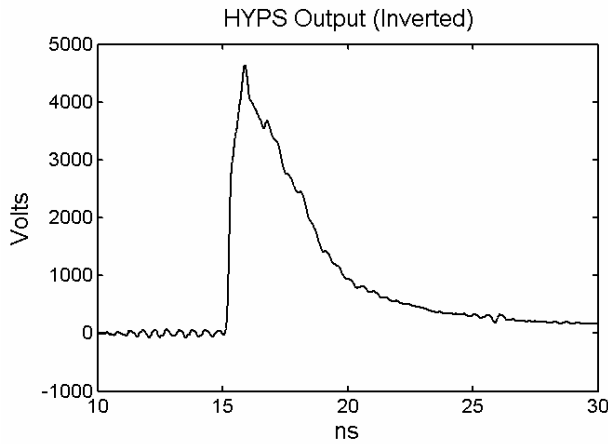


Figure 4.1. Output of the HYPS pulser.

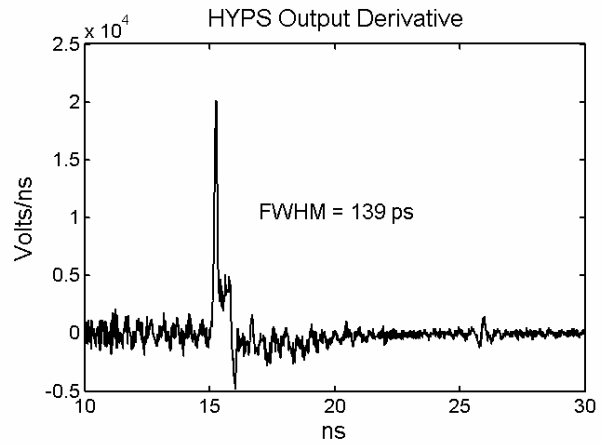


Figure 4.2. Derivative of the HYPS output.

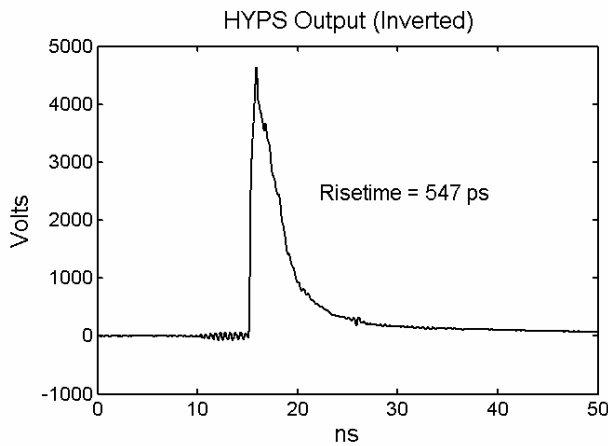


Figure 4.3. Output of the HYPS pulser.

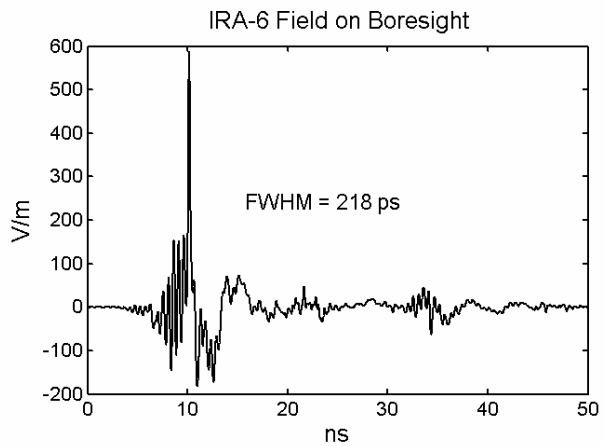


Figure 4.4. E field at 20.4m on boresight.

V. Higher Voltage Measurements

Finally, we tested the IRA-6 when driven by a higher voltage pulser, the FID model FPG 30-1KM. This unit has a peak voltage of around 30 kV and a risetime of 150 ps, according to the manufacturer's specifications. We begin by describing the characteristics of the pulser, and then we show the radiated field data.

We characterized the pulser with the experimental configuration shown in Figure 5.1. We surrounded the FPG with a grounded, screened enclosure. We fired the pulser through a Farr Research model VDC-1 V-dot cable sensor into a 54-ohm dummy load. We placed a 10.3-meter cable between the probe and the matched load, to reduce reflections. We used the internal trigger generator of the FPG operating at 1 kHz.

The raw output of the sensor is shown in Figure 5.2 on the left, and its integral is shown on the right. We find the FWHM of the derivative waveform to be 170 ps, and the FWHM of the integrated waveform to be 1.3 ns. The peak voltage is 25 kV.

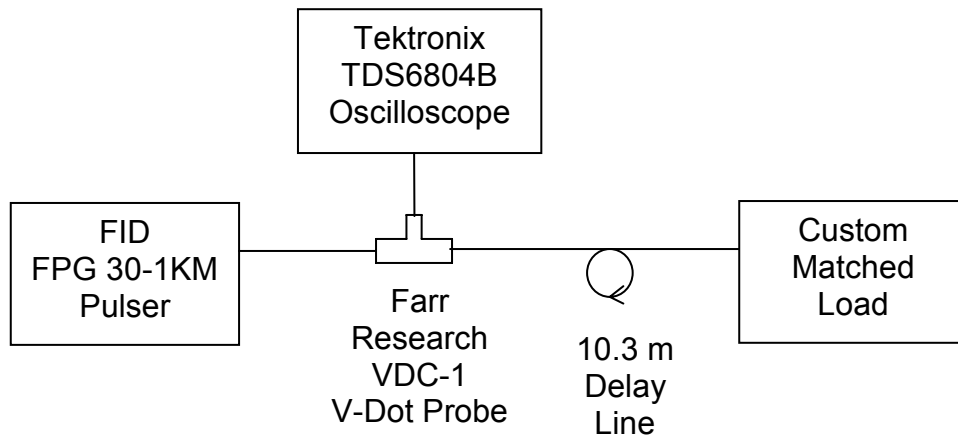


Figure 5.1. Equipment block diagram.

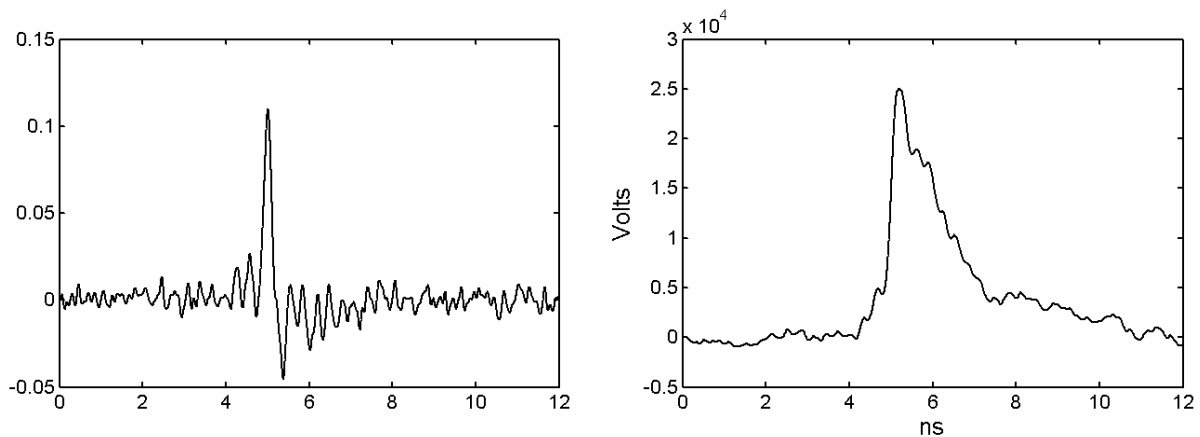


Figure 5.2. Raw data (left) and integrated data (right) for the FID model FPG 30-1KM pulser.

Having characterized the source, we then measured the radiated field when the FID pulser drives the IRA-6. We measured the field using a Farr Research model TEM-1-50 sensor ($h_{eff} = 0.018$ m) at a distance of 20.4 m, using a Tektronix model TDS6804 oscilloscope. There was a 2-meter cable of type RG 58 A/U between the sensor output and source, and the effect of this cable was not deconvolved from the data. The sensor was accounted for by a scalar correction factor, as in the previous section.

The results are shown in Figure 5.3, where we observe a peak radiated field of 2.8 kV/m, and a FWHM of 254 ps. Since we had already characterized the IRA-6 at low voltage, there was little new to be learned from this data. However, it was important to demonstrate the ability to drive the IRA-6 at 25 kV without any apparent flashover. We can observe from the data this was indeed the case.

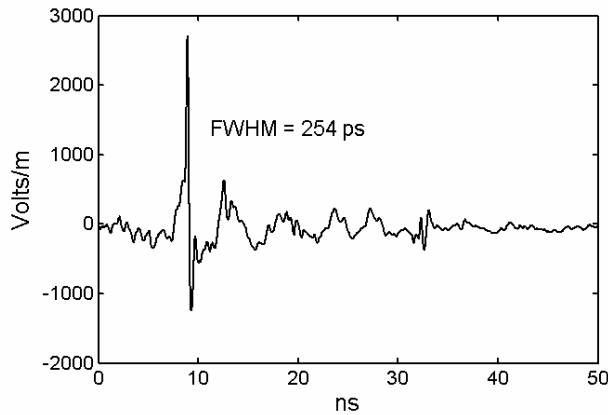


Figure 5.3. Field radiated from the IRA-6 when driven by the FID model FPG 30-1 KM pulser.

VI. Conclusions

We were successful in developing the IRA-6, which is a higher-voltage version of a cable-fed IRA with a Type-HN input connector, and with a diameter of 1.5 meters. This antenna was able to tolerate a peak voltage of 25 kV without flashover, and performed well up to 4 GHz. It is possible that the IRA-6 might be able to tolerate even higher voltages, but this was not tested. These characteristics were sufficient for the intended application of a UWB radar with directional coupler.

Further refinement of the splitter and feed point may lead to a flatter TDR, and improved risetime and realized gain. In radar applications, it is important that the TDR of an antenna be very flat, however, it becomes more challenging to achieve this at higher voltages. The TDR was very flat at the load resistors.

The peak realized gain of the IRA-6 was 20 dBi at 3.1 GHz. The peak measured E field at 20 m on boresight of the IRA-3 was 600 V/m when driven by a 4.5-kV pulser, and 2.8 kV/m with the 25-kV pulser.

Finally we found that the aluminum honeycomb material used in the feed arms and ground plane was very effective in reducing the weight of the antenna while maintaining strength and rigidity. The original design of the IRA-6 included some additional structural members that were not used because the honeycomb performed so well.

Acknowledgements

We are pleased to acknowledge many helpful discussions on this topic with Dr. Carl E. Baum, formerly with Air Force Research Laboratory, Directed Energy Directorate, and currently with University of New Mexico. We also wish to thank AFRL/DE for funding this work.

References

1. L. M. Atchley, E. G. Farr, D. E. Ellibee, and D. I. Lawry, "A High-Voltage UWB Coupled-Line Directional Coupler," Sensor and Simulation Note 489, April 2004.
2. L. H. Bowen, E. G. Farr, *et al*, Results of Optimization Experiments on a Solid Reflector IRA, Sensor and Simulation Note 463, January 2002.
3. L. H. Bowen, E. G. Farr, C. E. Baum, and W. D. Prather, "Experimental Results of Optimizing the Location of Feed Arms in a Collapsible IRA and a Solid IRA," Sensor and Simulation Note 450, November 2000.
4. E. G. Farr and L. H. Bowen, "The Relationship Between Feed Arm Position and Input Impedance in Reflector Impulse Radiating Antennas," Sensor and Simulation Note 499, April 2005.
5. L. M. Atchley, E. G. Farr, *et al*, "Characterization of a Time Domain Antenna Range," Sensor and Simulation Note 475, June 2003.
6. E. G. Farr and C. E. Baum, "Time Domain Characterization of Antennas with TEM Feeds," Sensor and Simulation Note 426, October 1998
7. E. G. Farr, "Optimizing the Feed Impedance of Impulse Radiating Antennas, Part I: Reflector IRAs," Sensor and Simulation Note 354, January 1993.